*J. Fluid Mech.* (1986), *vol.* 165, *pp.* 297–318
*Printed in Great Britain*



# Stability of lifted laminar round gas-jet flame

By Ö. SAVAŞ AND S. R. GOLLAHALLI

School of Aerospace, Mechanical and Nuclear Engineering, The University of Oklahoma, Norman, Oklahoma 73019, USA

(Received 27 June 1985 and in revised form 15 October 1985)

The exact solution of the concentration field of jet fluid in a round laminar jet is presented. This analytical solution, which assumes constant kinematic viscosity and molecular diffusivity, establishes the dependence of the concentration field on the Schmidt number. This solution and a kinematic argument are used to calculate the shape of the lifted flame front in a round laminar jet. The observed shape of the lifted laminar propane flame front is compared with the prediction of this formulation. A spatial-stability criterion of the flame is developed and applied to examine the stability of the lifted flame in the flow field of the round laminar jet. The laminar flame blowout height and the corresponding Reynolds number are calculated from the stability criterion. The predictions agree well with the experimental values. The flame blowout Reynolds number of laminar fuel jets of pure fuels discharging from round pipes with fully developed laminar flow is shown to be directly proportional to the pipe diameter. At blowout the fuel concentration in the vicinity of the flame is found to attain a constant value which lies between the lean flammability limit and the fuel concentration at which the laminar flame speed is maximum. This stability criterion is generalized to laminar gas-jet flames of different fuels using three experimentally determined parameters describing their flame speed–concentration characteristics. The general form can account for dilution of fuel jets with inert gases. That flames can be lifted and blown out while they are still laminar is also demonstrated experimentally.

## 1. Introduction

Although it was first studied over thirty years ago (Scholefield & Garside 1949; Barr 1953), the subject of the stability of gas diffusion flames has received considerable attention in recent years (Peters & Williams 1983; Broadwell, Dahm & Mungal 1985; Eickhoff, Lenze & Leuckel 1985; Peters 1985; Takahashi, Mizomoto, Ikai & Futaki 1985). All of these studies are concerned with turbulent flames and have dealt with several topics such as the liftoff mechanisms, liftoff height, jet velocities at which liftoff and blowout occur, and their hysteresis behaviour. An obvious first step in determining the mechanisms of stability of lifted turbulent jet flames is to understand the corresponding features in the laminar case. Little information, however, is available in the literature on the stability of lifted laminar gas-jet flames, presumably because it was thought that lifted flames could not be stabilized if the flame was laminar (Scholefield & Garside). Further, there are no rigorous studies to relate the fluid mechanics and flow pattern of the jet flames under transition conditions to the stability parameters. Hence, a research program on the stabilization mechanisms of jet flames under a wide range of conditions is currently underway in the authors' laboratory (Savaş & Gollahalli 1985), one phase of which forms the topic of this paper.

This paper deals with a theoretical and experimental study of the shape of the

reaction zone of a lifted flame of a laminar round jet and the development of a criterion for its spatial stability. It is a limiting case where the flame behaves like a premixed flame in the far field of a narrow tube and is thin in comparison to its radius of curvature and to distances over which the concentration and velocity gradients occur. The question of the existence of the flame is separated from that of its stability. The governing conservation equations are first solved for the flow and concentration fields of a round laminar jet. This exact solution, which is analogous to Squire's (1951) solution of the temperature field, displays explicitly the effect of the Schmidt number, which is often assumed to be unity for convenience in theoretical studies. Depending on the parameters of the flow configuration, there may be for the flame one solution, two solutions, or no solutions at all. The existence of a real solution suggests that a laminar flame can be maintained in the flow field. Then the solutions are examined for their spatial stability. In this analysis the question of whether the flame moves to its original configuration following a disturbance is examined and a stability criterion is proposed. A simplified form of this formal criterion is obtained for the stability of the flame to infinitesimal disturbances. The criterion of the existence of the flame in the far field is examined closely to deduce the conditions of the blowout of gas diffusion flames while they are entirely laminar. Experimental results are presented that verify the analysis developed in this article. In particular, it is demonstrated that a gas-jet flame can be lifted, stabilized downstream, and blown out in a laminar-jet flow field.

## 2. Flow field

One of the few exact solutions of the equations of motion of fluid flow is that of the laminar flow field of a point momentum source in an unbounded quiescent fluid in the absence of body forces. This solution is usually attributed to Squire (1951) even though Landau & Liftshitz (1959) refer the solution to Landau (1944). Some steps of this solution are outlined below for later use in the solution of the associated diffusion equation (see, for example, Batchelor (1967) for more details). The flow field is characterized by the momentum $J$ of the jet and the density $\rho_\infty$ and the kinematic viscosity $\nu_\infty$ of the ambient fluid. Thus, the Reynolds number $Re = (J/\rho_\infty)^{\frac{1}{2}}/\nu_\infty$ is the only parameter needed to describe the flow field uniquely. The jet is located at the origin of the reference system shown in figure 1 and aligned with the $x$-direction which is the axis of symmetry of the flow field. For convenience, both spherical polar coordinates, $\boldsymbol{x} = (R, \theta, \phi)$, and cylindrical polar coordinates, $\boldsymbol{x} = (r, \phi, x)$, are used. The flow has no swirl and no dependence on the azimuthal coordinate $\phi$. Thus, the velocity vector $\boldsymbol{u}(\boldsymbol{x})$ has two non-zero components $(u_R, u_\theta)$ or, equivalently, $(u_x, u_r)$ as defined in figure 1. The velocity vector is expressed in terms of the Stokes stream function $\psi(R, \theta)$ as

$$(u_R, u_\theta) = \left(\frac{1}{R^2 \sin\theta}\frac{\partial\psi}{\partial\theta}, -\frac{1}{R\sin\theta}\frac{\partial\psi}{\partial R}\right). \tag{1a}$$

The equations of motion yield an explicit analytic solution for the stream function in the form

$$\psi(R, \theta) = 2\nu_\infty R\frac{\sin^2\theta}{1+a-\cos\theta}. \tag{1b}$$

The constant $a$ is related to the momentum, and hence to the Reynolds number of the jet through

$$Re^2 = 8\pi\left[\frac{8}{3}\frac{1+a}{a(2+a)} + (1+a)^2\ln\left(\frac{a}{2+a}\right) + 2(1+a)\right]. \tag{1c}$$

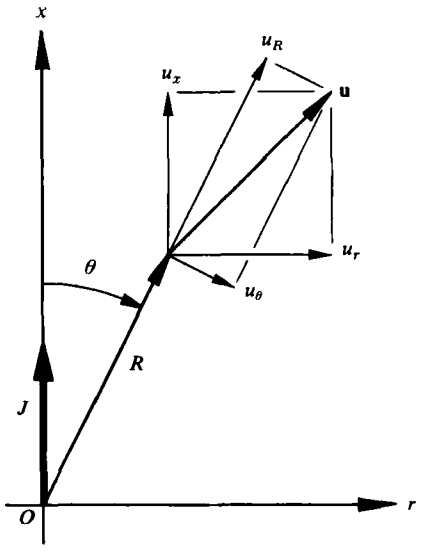


FIGURE 1. Definition of the coordinate systems and the components of the velocity vector.

Note that $a$ decreases monotonically with increasing Reynolds number. The asymptotic forms of (1$c$) for small and large Reynolds numbers are

$$Re \sim \left(\frac{16\pi}{a}\right)^{\frac{1}{2}} \quad \text{for } a \gg 1, \tag{1d}$$

and

$$Re \sim \left(\frac{32\pi}{3a}\right)^{\frac{1}{2}} \quad \text{for } a \ll 1. \tag{1e}$$

Also, for example, $a = 3.32 \times 10^{-3}$ at $Re = 100$. Further, the magnitude of the velocity vector $\boldsymbol{u}$ along the symmetry axis is

$$u_0(x) = \frac{4\nu_\infty}{ax}. \tag{1f}$$

The flow field can be described completely using single contours for the velocity components. For instance, the axial velocity component $u_x = u_R \cos\theta - u_\theta \sin\theta$ can be described as

$$u_x = \frac{4\nu_\infty}{aR_0} \tag{1g}$$

on the contour passing through $(R, \theta) = (R_0, 0)$ and given by

$$\frac{R}{R_0} = \tfrac{1}{2}a \frac{(1+a)(1+\cos^2\theta) - 2\cos\theta}{(1+a-\cos\theta)^2}. \tag{1h}$$

Figure 2 shows the $u_x$ contours for Reynolds numbers of 10, 100, and 200. There is a substantial induced motion upstream of the origin at low Reynolds numbers (figure 2$a$). For later comparison with the corresponding concentration field, note that the limit of the contour (1$h$) for $\theta \ll 1$ is

$$\frac{R}{R_0} = \frac{a^2}{(1+a-\cos\theta)^2}. \tag{1i}$$

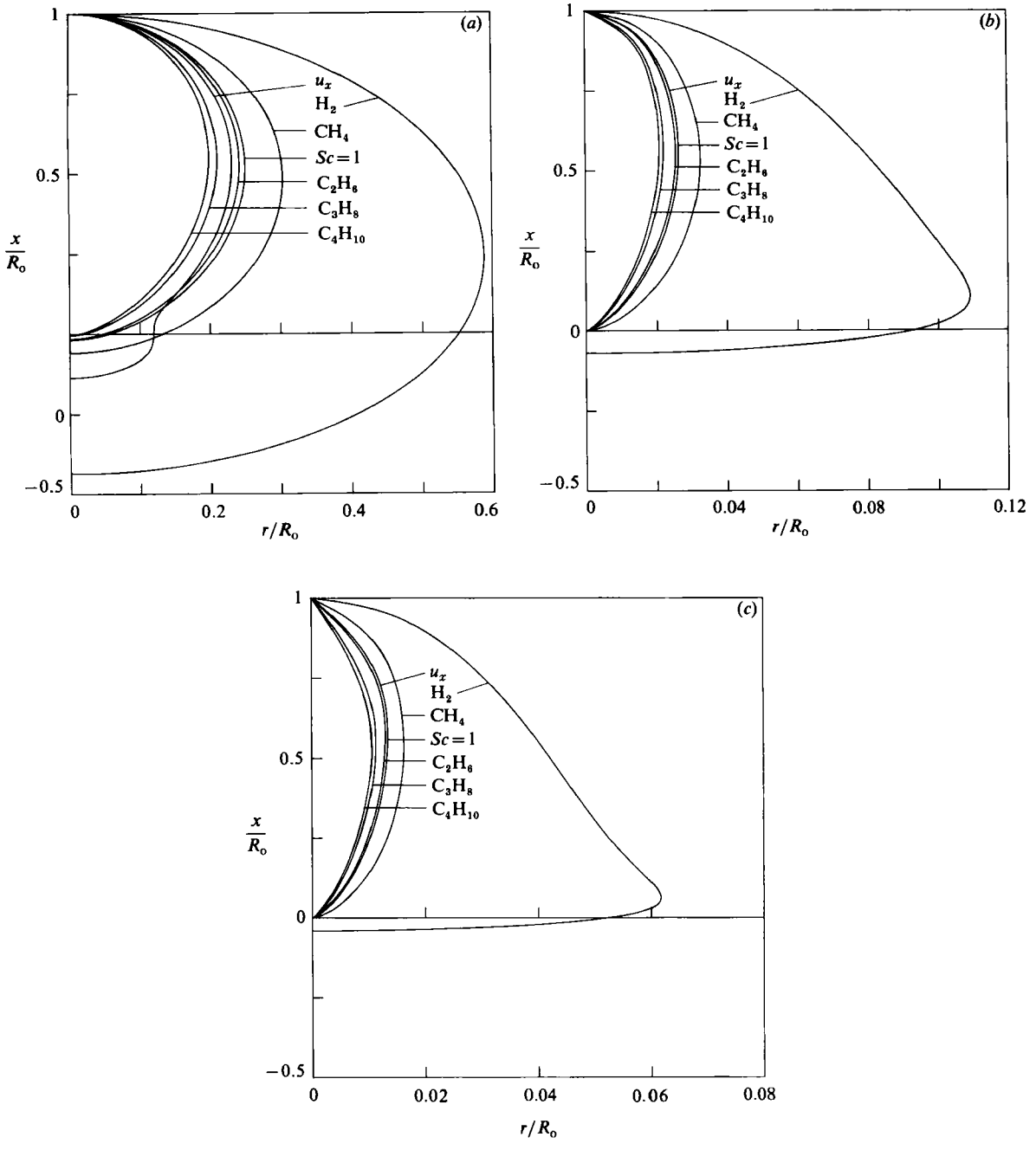


FIGURE 2. Velocity and concentration contours in round laminar jet. The concentration contours are drawn for hydrogen, methane, ethane, $Sc = 1$, propane, and butane jets in air. Note that the expanded $r$ scale distorts the contours, especially, around $x = 0$ plane. (*a*) $Re = 10$, (*b*) $Re = 100$, and (*c*) $Re = 200$.

## 3. Concentration field

The concentration field associated with the laminar round jet can be determined exactly from the solution of the diffusion equation

$$\boldsymbol{u}(\boldsymbol{x})\cdot\operatorname{grad} C(\boldsymbol{x}) = D \operatorname{div}\operatorname{grad} C(\boldsymbol{x}), \tag{2}$$

where $\boldsymbol{u}(\boldsymbol{x})$ is the velocity field given by (1), $D$ is the coefficient of binary diffusion into the surrounding medium of the species emanating from the origin, and $C(\boldsymbol{x})$ is the molar concentration of the diffusing species. Both the kinematic viscosity and the molecular diffusivity are assumed to be constants. We also assume that the density variations in the flow field due to $C(\boldsymbol{x})$ are low enough so that (1) remains as an acceptable approximation of the velocity field $\boldsymbol{u}(\boldsymbol{x})$ in (2). The solution of (2) is given by Squire in the context of the temperature field of a heated laminar round jet. This elegantly simple solution exploits the property that the concentration field can be written as $C(R,\theta) = g(\theta)/R$, where $g(\theta)$ is determined from (2). The solution with the proper boundary condition $\partial C/\partial\theta = 0$ at $\theta = 0$ is

$$C(R,\theta) = \frac{b}{R(1+a-\cos\theta)^{2Sc}}, \tag{3a}$$

where $Sc \equiv \nu_\infty/D$ is the Schmidt number and $b$ is a constant determined from the source strength at the origin. The concentration along the centreline of the jet is

$$C_0(x) = \frac{b}{a^{2Sc}x}, \tag{3b}$$

and has the same $x$ dependence as the centreline velocity $u_0(x)$ (cf. (1$f$)). If $N$ moles of the species are introduced per unit time at the origin into the flow field, then $b$ is determined from the species conservation integral

$$N = \iint_A C(\boldsymbol{x})\,\boldsymbol{u}(\boldsymbol{x})\cdot\mathrm{d}\boldsymbol{A},$$

where $\mathrm{d}\boldsymbol{A}$ is the differential vector surface element and the integration is done over any closed surface $A$ around the origin. This calculation yields

$$b = \frac{N}{8\pi\nu_\infty}\frac{4Sc^2-1}{(2Sc+1+a)(2+a)^{-2Sc}+(2Sc-1-a)a^{-2Sc}}. \tag{3c}$$

A useful limit of (3$c$) is for high Reynolds number

$$b \sim \frac{N}{8\pi\nu_\infty}(2Sc+1)a^{2Sc} \quad \text{for } Re \gg 1. \tag{3d}$$

Note that (3$c$) needs to be handled with some care for $Sc = \frac{1}{2}$.

Analogous to the velocity field, the concentration field for a given Reynolds number can be shown graphically using one contour only as

$$C = \frac{b}{a^{2Sc}R_0} \quad \text{on} \quad \frac{R}{R_0} = \frac{a^{2Sc}}{(1+a-\cos\theta)^{2Sc}}. \tag{3e,f}$$

The shape of the concentration contour is determined by the Reynolds number of the jet and the Schmidt number and is independent of the molar flux $N$. Velocity and concentration contours (1$h$) and (3$f$) for the laminar jets are shown together in

figure 2. The figure shows the velocity contour $u_x$ and six concentration contours for $Re = 10$, 100, and 200 and for $Sc = 1.524$, 1.376, 1.0, 1.062, 0.704, and 0.204. The concentration contour corresponding to $Sc = 1$ is nearly the same as the velocity contour, especially at high Reynolds numbers and for $\theta \ll 1$, and is of only academic interest. The other five concentration contours are, however, drawn for Schmidt numbers corresponding to diffusion of butane, propane, ethane, methane, and hydrogen into air. The relative positions of these contours with respect to the velocity contour are important in the analysis of the flames of these gases in air as discussed below. Due to their high molecular diffusivities, hydrogen and to some extent methane diffuse upstream beyond the jet origin. The solution of (2) within the usual boundary-layer approximation cannot account for this behaviour, and, therefore, due caution must be exercised in extending such solutions to the description of fields with low Schmidt numbers. It should be noted from (1*d*) and (3) that, as the Reynolds number approaches zero, the concentration field tends to that of the radial diffusion from a point source in quiescent surroundings and the concentration contours tend to the sphere $R/R_0 = 1$.

## 4. Lifted flame front

We take (1) and (3) as the solutions of the velocity and concentration fields in the far field of a fuel jet issuing into a quiescent oxidizer, such as propane jet discharging from a small tube of diameter $d$ into air. Such an approximation is restricted to sufficiently low Reynolds numbers so that thc jet flow is laminar and to regions of the flow where $R/d \gg 1$ so that flow is in its asymptotic form described by (1).

The lifted laminar flame over a small-diameter tube burner offers an example of such a flow field. In particular, the shape of the lifted flame front can be calculated from the velocity and concentration fields given by (1) and (3). On the flame surface $F(\theta)$ the local laminar flame speed $u_f$, defined as the speed relative to unburnt gas of a plane flame front along the normal to its surface, is equal to the component of the local velocity vector normal to the flame surface (figure 3). Thus, we determine the shape of the flame front from the kinematic condition that

$$\boldsymbol{u}(\boldsymbol{x})\cdot\boldsymbol{n}(\boldsymbol{x}) = u_f(\boldsymbol{x}), \tag{4a}$$

where $\boldsymbol{n}(\boldsymbol{x})$ is the unit normal vector to the flame front as indicated in figure 3. The unit normal vector $\boldsymbol{n} = (n_R, n_\theta)$ can be expressed in terms of the equation of the flame front $F(\theta)$ as

$$\boldsymbol{n}(\boldsymbol{x}) = \frac{[1, -\mathrm{d}\ln F/\mathrm{d}\theta]}{[1+(\mathrm{d}\ln F/\mathrm{d}\theta)^2]^{\frac{1}{2}}}. \tag{4b}$$

Substitution of (4*b*) into (4*a*) and incorporation of (1) gives the following first-order ordinary differential equation for the flame front $F(\theta)$:

$$\frac{\mathrm{d}F_\pm}{\mathrm{d}\theta} = F_\pm \frac{-\frac{u_R}{u_f}\frac{u_\theta}{u_f} \pm \left[\left(\frac{u_R}{u_f}\right)^2 + \left(\frac{u_\theta}{u_f}\right)^2 - 1\right]^{\frac{1}{2}}}{1-\left(\frac{u_\theta}{u_f}\right)^2}. \tag{4c}$$

We have assumed that the presence of the flame does not change the upstream flow and concentration fields significantly. There are two distinct solutions, $F_+(\theta)$ and $F_-(\theta)$, corresponding to the two signs of the radical in (4*c*). They are discussed below for propane flame and $F_+(\theta)$ is chosen as the proper solution. The velocity components

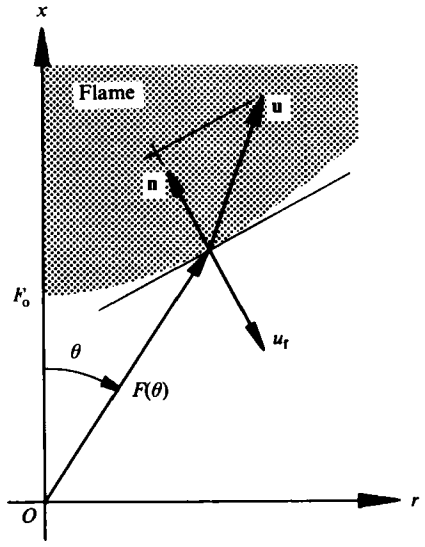


FIGURE 3. Flame front. Note that the normal unit vector $\boldsymbol{n}$ points into the flame.

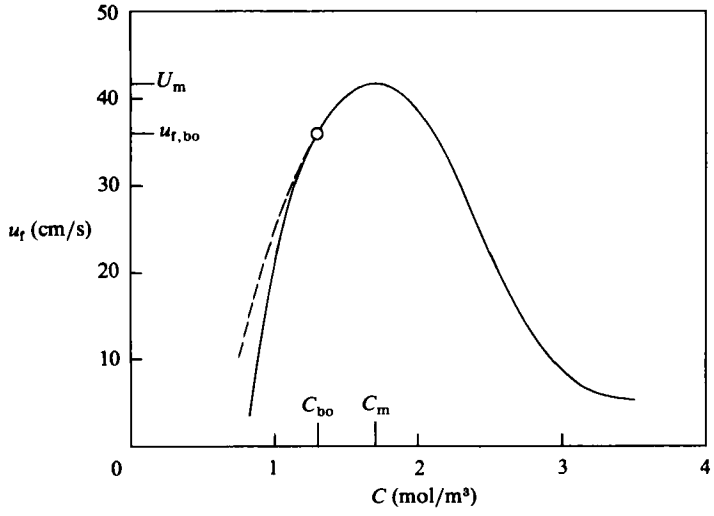


FIGURE 4. Flame speed $u_f$ versus molar concentration $C$ for propane–air mixture. ——, cubic spline fit to data from Egerton & Thabet (1952) and Botha & Spalding (1954); – – – –, (10) with $(U_m, C_m, \alpha) = (41.7 \text{ cm/s}, 1.70 \text{ mole/m}^3, 2.41)$; ○, blowout condition.

$u_R$ and $u_\theta$ depend on $R$ and $\theta$ and are available from (1). The flame speed $u_f$ is often a complicated function of numerous variables such as concentration, temperature, and pressure (depending on the order of the combustion reaction). For the calculation of the shape of the lifted flame front to compare with the flame in laboratory conditions (i.e. constant pressure and temperature), we assume the $u_f$ is mainly determined by the concentration field upstream of the flame front and neglect the other effects. The laminar flame velocity $u_f$ is considered insensitive to pressure as most hydrocarbon–air combustion reactions are of second order. Neglecting the effect of the buoyancy through the presence of the flame is, perhaps, as serious an

assumption as neglecting the heat losses from the flame front to the surroundings. The concentration field is available from (3) as a function of $R$ and $\theta$. What is needed now is a usable relation between $C$ and $u_f$, namely, $u_f = u_f(C)$. Such a functional relationship may be available either theoretically or experimentally (e.g. figure 4). The boundary condition of (4$a$) is determined from the behaviour of $F(\theta)$ along the $x$-axis. No cusp is allowed on the symmetry axis, thus $\partial F/\partial\theta = 0$ at $\theta = 0$. It follows from (4$c$) that, at $F_0 = F(0)$, $u_f = u_R$. When (1) and (3) are incorporated, the boundary condition of (4$c$) is established as

$$F = F_0 \quad \text{at} \quad \theta = 0$$

such that

$$\frac{4\nu}{aF_0} = u_f(C(F_0)),$$

$$= u_f\left(\frac{b}{a^{2Sc}F_0}\right). \tag{4d}$$

This algebraic equation may be solved either analytically or numerically depending on the available form of $u_f(C)$. Equation (4$d$) may have a single solution, two distinct solutions, one double solution, or no solution at all. A solution of (4) is discussed below in detail for a propane jet.

## 5. Stability

Once the shape of the flame front $F(\theta)$ and its normal $\boldsymbol{n}(\theta)$ are calculated from (4), what remains to be done is to establish if the solution is spatially stable. We do not address here the question of thermodiffusive instabilities such as those summarized by Sivashinsky (1983). We define a stable flame as one which tends to its original configuration when disturbed. In differential terms, subsequent to the displacement $\mathrm{d}\boldsymbol{x}$ of an infinitesimal element of a disturbed flame front, the new balance between the local flame speed $u_f + \mathrm{d}u_f$ and the component of the local velocity vector normal to the flame surface $\boldsymbol{u}\cdot\boldsymbol{n} + \mathrm{d}(\boldsymbol{u}\cdot\boldsymbol{n})$ decide the stability of the flame. That the differential increment $\mathrm{d}(u_f - \boldsymbol{u}\cdot\boldsymbol{n})$ has a net balance toward the original flame element is sufficient for the flame to return to its original configuration, therefore, be stable. This requirement may be mathematically expressed as

$$\mathrm{d}(u_f - \boldsymbol{u}\cdot\boldsymbol{n})\,(\mathrm{d}\boldsymbol{x}\cdot\boldsymbol{n}) \geqslant 0, \tag{5a}$$

which is written as

$$[\mathrm{d}\boldsymbol{x}\cdot\mathrm{grad}\,(u_f - \boldsymbol{u}\cdot\boldsymbol{n})]\,(\mathrm{d}\boldsymbol{x}\cdot\boldsymbol{n}) \geqslant 0, \tag{5b}$$

and expanded subsequently as

$$(\mathrm{d}\boldsymbol{x}\cdot\mathrm{d}\boldsymbol{x})\,[\boldsymbol{n}\cdot\mathrm{grad}\,(u_f - \boldsymbol{u}\cdot\boldsymbol{n})] - (\mathrm{d}\boldsymbol{x}\times\boldsymbol{n})\cdot[\mathrm{d}\boldsymbol{x}\times\mathrm{grad}\,(u_f - \boldsymbol{u}\cdot\boldsymbol{n})] \geqslant 0. \tag{5c}$$

In the special case of the infinitesimal displacement of the flame normal to itself, (5$c$) simplifies to

$$\boldsymbol{n}\cdot\mathrm{grad}\,(u_f - \boldsymbol{u}\cdot\boldsymbol{n}) \geqslant 0. \tag{6a}$$

We take this condition as the criterion of stability of a flame front to infinitesimal disturbances. This criterion combines together the flame shape $\boldsymbol{n}(\boldsymbol{x})$, the flow field $\boldsymbol{u}(\boldsymbol{x})$, and, through $u_f = u_f(C)$, the concentration field $C(\boldsymbol{x})$. Note that the left-hand side of (6$a$) is the derivative of $(u_f - \boldsymbol{u}\cdot\boldsymbol{n})$ normal to the flame front and into the flame;

$$\frac{\mathrm{d}}{\mathrm{d}n}(u_f - \boldsymbol{u}\cdot\boldsymbol{n}) \geqslant 0. \tag{6b}$$

The role of the concentration field may be better seen if (6*a*) is expanded as

$$\boldsymbol{n}\cdot\left[\frac{\mathrm{d}u_{\mathrm{f}}}{\mathrm{d}C}\,\mathrm{grad}\,C-\mathrm{grad}\,(\boldsymbol{u}\cdot\boldsymbol{n})\right]\geqslant 0. \tag{6c}$$

The derivative $\mathrm{d}u_{\mathrm{f}}/\mathrm{d}C$ may be available experimentally from data such as shown in figure 4.

A simpler form of (6*c*) is obtained if a one-dimensional flame field is considered. Since $\boldsymbol{x}$ and $\boldsymbol{n}$ are in the same direction the gradients become ordinary derivatives and (6*c*) reduces to

$$\frac{\mathrm{d}u_{\mathrm{f}}}{\mathrm{d}C}\frac{\mathrm{d}C}{\mathrm{d}x}-\frac{\mathrm{d}u}{\mathrm{d}x}\geqslant 0, \tag{7}$$

where $u$ is the flow velocity which points in the positive $x$-direction, and the flame is propagating in the negative $x$-direction. Note that, in the case of the neutrally stable flame front of one-dimensional premixed flame propagating normal to itself, both $\mathrm{d}C/\mathrm{d}x$ and $\mathrm{d}u/\mathrm{d}x$ are zero and (7) holds with the equality sign, confirming the neutral stability of such a flame front. In other words, such a propagating flame front has no preference in space as long as the conditions are uniform and the fuel concentration is within the flammability limits. The application of (7) to the lifted flame in the laminar round jet is presented below.

In the case of analysing the general stability of a flame, the displacement $\mathrm{d}\boldsymbol{x}$ of the flame changes both the velocity and the concentration fields. Therefore, the rigorous application of the stability criterion (5) may require considerable effort. In particular, the changes in the flow and concentration fields may be to such an extent that the flame may move to a different location which is stable to infinitesimal disturbances but not to large disturbances. The hysteresis phenomenon observed in the diffusion flames over burners is one such case where the flame is stable to infinitesimal disturbances, but can be forced to lift off or reattach by sufficiently intense forcing (see, for example, Scholefield & Garside and, for a more recent example, Savaş & Gollahalli).

In the case of the solution from (4) of the lifted flame front of the laminar round jet, it is sufficient to investigate the stability of the flame front along the $x$-axis. The flame is stable, when moved slightly downstream, the local flow velocity should be lower than the local flame velocity so that the flame can move upstream to its original position, and, when moved slightly upstream, the local flow velocity should be higher than the local flame velocity so that the flame can be lifted back to its original position. In quantitative terms, this requirement is equivalent to $\mathrm{d}u_{\mathrm{f}}/\mathrm{d}x\geqslant \mathrm{d}u_x/\mathrm{d}x$ along the $x$-axis. Equality holds for neutral stability. Using the chain rule of differentiation, this expression is written as

$$\frac{\mathrm{d}u_{\mathrm{f}}}{\mathrm{d}C}\frac{\mathrm{d}C}{\mathrm{d}x}\geqslant\frac{\mathrm{d}u_x}{\mathrm{d}x}. \tag{8a}$$

This expression is derived from purely intuitive arguments and is identical to the one-dimensional stability criterion expressed in (7), which is deduced from the general stability hypothesis (5). The two spatial derivatives $\mathrm{d}C/\mathrm{d}x$ and $\mathrm{d}u_x/\mathrm{d}x$ are available from (3) and (1), respectively. The expression simplifies to

$$\frac{\mathrm{d}u_{\mathrm{f}}}{\mathrm{d}C}\leqslant\frac{4\nu_\infty a^{2Sc-1}}{b}. \tag{8b}$$

The right-hand side of this inequality is positive; therefore any flame located on the rich-flammability branch of $u_f(C)$ curve is stable. Flames are stable only on the portion of the lean-flammability branch adjacent to the maximum flame speed.

## 6. Blowout

The existence of solutions of (4*d*) deserves close attention. As the Reynolds number increases, the unstable and the stable solutions move close to each other. The two solutions coincide when the local flame velocity and the fluid velocity and their derivatives are equal. Now, (7) and (8) become equalities. Beyond this critical Reynolds number $Re_{bo}$, (4) has no solutions for the flame front; therefore, the jet can no longer sustain a free flame. We define this condition as the blowout condition of the round laminar flame. The blowout parameters, namely the flame liftoff height at blowout $x_{bo}$ and the blowout Reynolds number $Re_{bo}$, are determined from the simultaneous solutions of

$$u_x(x) = u_f(x), \tag{9a}$$

and

$$\frac{du_x}{dx} = \frac{du_f}{dx}. \tag{9b}$$

These two equations can in principle be solved simultaneously to obtain the useful parameters $Re_{bo}$ and $x_{bo}$. An exact analytical solution requires a usable form of the flame speed as a function of the concentration $u_f(C)$. Most of the available information is in the form of experimental data which show considerable scatter depending on the particular measurement technique used. The solution of (9) occurs on the lean branch of the $u_f(C)$ curve near the maximum flame velocity (cf. inequality (8*b*)). Therefore, a parabola approximating the lean branch of the experimental data is well suited for the solution of the blowout conditions. The functional form of this curve fit is

$$\frac{u_f}{U_m} = 1-\alpha\left(1-\frac{C}{C_m}\right)^2. \tag{10}$$

The two parameters $U_m$ and $C_m$ are the maximum flame velocity and the corresponding molar concentration, which are fixed values for a given fuel–oxidizer combination. Therefore, the only adjustable parameter of the curve fit is $\alpha$, which is larger than unity for common fuel–oxidizer pairs. For convenience, we define another parameter $\beta \equiv 1-(1-1/\alpha)^{\frac{1}{2}}$ such that $0 < \beta < 1$. Typical values of these four parameters for some fuels are presented in table 1. Considering the scatter in the available data, the error introduced in this approximation is within the uncertainty of data.

By using (1*e*), (3*d*), and (10) the solution of the blowout condition (9) for large Reynolds number ($Re \gg 1$) is obtained as

$$\frac{U_m x_{bo}}{\nu_\infty} = \frac{1}{8\pi}\frac{2Sc+1}{1-\beta}\frac{U_m N_{bo}}{\nu_\infty^2 C_m}, \tag{11a}$$

and

$$Re_{bo}^2 = \tfrac{2}{3}\alpha\beta(2Sc+1)\frac{U_m N_{bo}}{\nu_\infty^2 C_m}, \tag{11b}$$

where $N_{bo}$ is the molar fuel flow rate at blowout. The local concentration $C_{bo}$ at $x_{bo}$ is determined from (3*b*) as

$$C_{bo} = (1-1/\alpha)^{\frac{1}{2}} C_m, \tag{11c}$$

| Fuel | | Molecular mass $M_f$ (g/mole) | Schmidt number $Sc$ | Density $\rho_f$ (kg/m$^3$) | Maximum flame speed $U_m$ (cm/s) | Concentration at $U_m$ $C_m$ (mole/m$^3$) | $\alpha$ | $\beta$ | $\gamma$ (mm$^{-1}$) | $\delta$ (mm$^{-1}$) | Reference |
|---|---|---|---|---|---|---|---|---|---|---|---|
| Hydrogen | $H_2$ | 2.016 | 0.204 | 0.0833 | 313 | 17.6 | 3.55 | 0.152 | 320 | 720 | Takahashi, Mizomoto & Ikai (1983) |
| Methane | $CH_4$ | 16.04 | 0.704 | 0.663 | 45.0 | 4.10 | 9.00 | 0.0574 | 270 | 255 | Andrews & Bradley (1972) |
| Ethane | $C_2H_6$ | 30.07 | 1.062 | 1.243 | 47.6 | 2.62 | 4.78 | 0.111 | 670 | 410 | Gibbs & Calcote (1959) |
| Propane | $C_3H_8$ | 44.11 | 1.376 | 1.824 | 41.7 | 1.70 | 2.41 | 0.235 | 1650 | 577 | Botha & Spalding (1954) |
| Butane | $C_4H_{10}$ | 58.12 | 1.524 | 2.403 | 44.9 | 1.32 | 3.17 | 0.172 | 2400 | 735 | Gibbs & Calcote (1959) |

TABLE 1. Flame parameters for some pure gaseous fuels burning in air at 730 torr and 20 °C

which is a sole property of the laminar flame speed characteristics of the particular fuel–oxidizer pair and independent of any other flow or fluid properties for the laminar round jet. The critical parameters of the flame are, thus, determined by the laminar flame speed characteristics $u_f(C)$ and the two dimensionless numbers; the Schmidt number and $U_m N_{bo}/\nu_\infty^2 C_m$, which is a measure of the fuel flux. Note that the location of the maximum flame velocity $U_m(C_m)$ would be at $x = (1-\beta)\, x_{bo}$. The flame liftoff distance at blowout $x_{bo}$ may be expressed conveniently in terms of the blowout Reynolds number as

$$\frac{U_m x_{bo}}{\nu_\infty} = \frac{3}{16\pi} \frac{1}{\alpha\beta(1-\beta)} Re_{bo}^2. \tag{11d}$$

These results show explicitly the dependence of the blowout parameters on the intrinsic properties of the particular fuel–oxidizer combination $U_m$, $C_m$, $\alpha$, $\nu_\infty$, and $Sc$; and the fuel flow rate $N_{bo}$. For a given fuel–oxidizer pair such as propane in air, the blowout Reynolds number $Re_{bo}$ depends on the square root of the molar fuel flow rate and the blowout height is directly proportional to the fuel flow rate.

The restrictive assumptions regarding the effects of the presence of the flame on the flow upstream of the flame front are no longer needed. At or near blowout, the flame is already extinct or near extinction; hence its upstream effects are no longer restrictions to the blowout parameters calculated in (11). Thus, for the laminar flame, the blowout has been accounted for by fluid-mechanics considerations using an intrinsic property of the fuel–oxidizer mixture $u_f(C)$ and without any additional reference to the chemical reactions in the flow field.

## 7. Experiments

### 7.1. *General remarks*

The jet momentum $J$ and the molar fuel flow rate $N$ are the two parameters needed to uniquely construct from (1) and (3) the flow field for a given gas jet in the laboratory. For the solution to be strictly applicable, $J$ should be introduced into the flow field with no mass flux and $N$ with no momentum. Neither can be achieved in practice. An acceptable approximation in the far field is obtained if the jet emerges from a small orifice. In such an experiment, however, the two parameters $J$ and $N$ are no longer independent. In particular, if the jet fluid of density $\rho_j$ and volumetric flow rate $Q_j$ is emerging from a small tube of diameter $d$ with a parabolic velocity profile, then

$$J = \left(\frac{16}{3\pi}\right)\left(\frac{\rho_j Q_j^2}{d^2}\right), \tag{12a}$$

$$Re = \left(\frac{16}{3\pi}\right)^{\frac{1}{2}}\left(\frac{\rho_j}{\rho_\infty}\right)^{\frac{1}{2}} \frac{Q_j}{\nu_\infty d}, \tag{12b}$$

and

$$N = \frac{\rho_f Q_j}{M_f}, \tag{12c}$$

where $\rho_f$ and $M_f$ are the partial density and the molar mass of the fuel carried by the jet fluid. Thus, $Q_j$ is the only flow parameter needed to ascertain $a$ and $b$ uniquely through (1$c$) and (3$b$). The blowout parameters for the flame over the tube are from (11$a$) and (11$b$),

$$\frac{U_m x_{bo}}{\nu_\infty} = \frac{1}{64} \frac{\alpha\beta}{1-\beta} (2Sc+1)^2 (\rho_\infty \rho_f)\left(\frac{U_m d}{\nu_\infty M_f C_m}\right)^2, \tag{13a}$$

and
$$Re_{\rm bo} = \frac{(3\pi)^{\frac{1}{2}}}{6}\alpha\beta(2Sc+1)\,(\rho_\infty \rho_{\rm f})^{\frac{1}{2}}\frac{U_{\rm m}\,d}{\nu_\infty M_{\rm f} C_{\rm m}}. \tag{13b}$$

Thus, the blowout conditions are related to fuel–oxidizer properties and the burner diameter $d$. The density $\rho_{\rm f}$ is the partial density of the fuel in the jet fluid, which is equal to that of the pure fuel gas if the fuel is not diluted. If the fuel is diluted with gases whose presence does not change the $u_{\rm f}(C)$ characteristics, then $\rho_{\rm f}$ is the conventional partial density of fuel gas in the mixture. Note that the Reynolds number of the flow in the tube and that of the jet differ from each other by the factor $(16/3\pi)^{\frac{1}{2}}(\rho_{\rm j}/\rho_\infty)^{\frac{1}{2}}$ and by the two different viscosities used. For example, a discharge flow rate of $Q = 0.653$ cm$^3$/s of propane into air through a tube of diameter $d = 0.353$ mm produces a jet Reynolds number of $Re = 200$, and the constants $a = 8.35\times10^{-4}$ and $b = 8.75\times10^{-14}$ mole/cm$^2$. An indirect way of controlling the two parameters $J$ and $N$ is to dilute the jet fluid. This method, however, is capable of producing only values of $N$ lower than the maximum value determined by the injection of pure fuel. The highest value of $N$ with the lowest value of $J$ may be achieve if the jet is discharged from the orifice with a uniform velocity. The construction of such an orifice to operate at flow rates low enough for laminar jet flow, however, may not be feasible owing to the rather thick boundary layers developing on the inside walls.

For a given fuel–oxidizer pair, the parameters for a laminar flame at blowout $x_{\rm bo}$ and $Re_{\rm bo}$ may be conveniently written as

$$x_{\rm bo} = \gamma d^2, \tag{14a}$$

and
$$Re_{\rm bo} = \delta d, \tag{14b}$$

where the dimensional constants $\gamma$ and $\delta$ are defined in (13$a$) and (13$b$) and are listed in table 1 for some pure fuel jets in air.

It is interesting to observe from (13$a$) that one needs to measure only the flame stand-off distance at blowout $x_{\rm bo}$ as a function of the tube diameter $d$ to test the validity of the arguments presented in this paper. In the following examples of flames, vertical fuel gas jets were produced in a quiet room over fine stainless-steel tubes of various sizes. Typical laboratory conditions were 730 torr atmospheric pressure and 20 °C room temperature. The tubes had internal diameters of 0.208, 0.353, and 0.432 mm. The tubes were typically a few centimetres long, ample to allow fully developed laminar flow at the Reynolds numbers investigated here. The ends were ground square and deburred. The flow rate was measured using a fine rotameter with a range of 0–1.5 cm$^3$/s (Gilmont, size no. 10). The direct and schlieren pictures were taken with a 35 mm camera. A brief description of the schlieren system may be found in Savaş & Gollahalli.

### 7.2. *Propane flame*

Propane jet in air offers a readily accessible way of testing the ideas developed above. The flame speed $u_{\rm f}(C)$ needed for the solution of (4) for the shape of the lifted flame front is experimentally available for propane–air mixture and is shown in figure 4. The data are taken from Egerton & Thabet (1952) and Botha & Spalding (1954). The fitted smooth curve is a third-order spline and is used in the numerical solution of (4). Note that there is no sustained flame beyond the flammability limits of propane. These limits are about $C_{\rm lean} = 0.83$ mole/m$^3$ and $C_{\rm rich} = 3.50$ mole/m$^3$ at typical laboratory conditions.

The first step in the solution of the lifted flame shape is to solve (4$d$) for the location

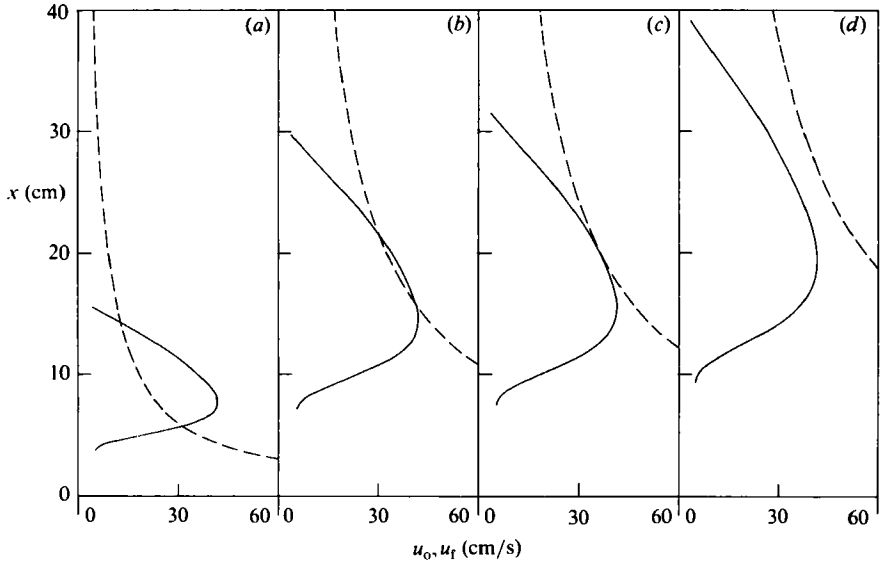


FIGURE 5. – – –, Axial velocity $u_o$ and ——, local flame velocity $u_f$ along the axis of the round laminar propane jet issuing from 0.353 mm diameter tube. (*a*) Lifted flame, below the critical Reynolds number, $Re = 100$. Stable solution in rich mixture. (*b*) Lifted flame, below the critical Reynolds number, $Re = 190$. Stable solution in lean mixture. (*c*) Lifted flame at the critical Reynolds number $Re_{bo} = 201.4$. (*d*) No flame, beyond the critical Reynolds number, $Re = 250$.

$R_o$ of the flame front on the axis of the jet. Four cases are shown in figure 5 for the 0.353 mm diameter tube. Each of the figures displays the axial velocity along the centreline $u_x$ and the flame velocity $u_f$ corresponding to the local concentration of propane.

There are two distinct solutions at sufficiently low Reynolds numbers. Either one (figure 5*a*) or both solutions (at higher Reynolds number) can be on the lean branch of the $u_f(C)$ curve of figure 4 (figure 5*b*). The appropriate choice between these two solutions is dictated by the stability criterion (7) (or, equivalently, (8*a*)). The larger of the two solutions is unstable, thus, cannot be realized in a conventional laboratory environment. Its existence may, however, be demonstrated experimentally in the laboratory. There is no flame if a small ignition source such as a match or a glowing filament is held over the fuel jet above the lean flammability limit. As the ignition source is lowered gradually to within the flammable-mixture region, a stable flame attached to the ignition source is observed. This flame moves up and disappears when the ignition source is moved radially away from the jet axis. If the source is moved further upstream below the location of the unstable solution, the flame moves and stabilizes at the axial location given by the stable solution. This behaviour is the direct consequence of stability arguments presented earlier, and summarized in (7) and (8*a*). Note that the stable flame position is not necessarily at the maximum possible flame speed for the fuel–air mixture.

As the flow rate $Q_j$ increases, therefore, the Reynolds number is increased, both solutions move downstream and approach each other. Eventually, the axial velocity curve and the local flame velocity curve become tangent to each other as shown in figure 5(*c*). Any further increase in flow rate causes extinction of the flame or, in conventional terms, blowout (Kanury 1977, p. 206). There is no self-sustaining flame

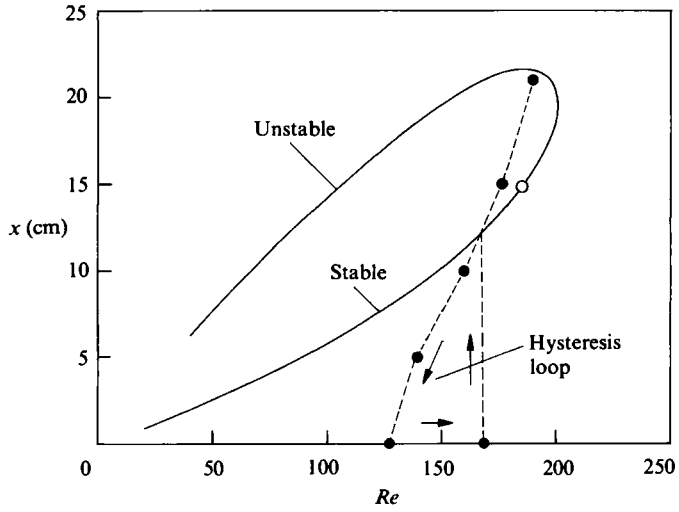


FIGURE 6. ——, Calculated and, ●, some measured values of the propane flame stand-off distance over the 0.353 mm diameter burner; ○, $u_o = U_m$. Note that there is no solution beyond the critical Reynolds number $Re_{bo} = 201$.

beyond this critical Reynolds number, which is calculated as $Re_{bo} = 201$ corresponding to $x_{bo} \approx 20$ cm for a tube with $d = 0.353$ mm. This critical flow condition corresponds to the equality of (8*b*). Note from figure 5(*c*) that the local concentration of propane drops below its lean flammability limit at a substantially higher location than $x_{bo}$.

At much higher flow rates, the $u_f$ and $u_x$ curves have no intersection, thus no solution for (4*b*) as shown in figure 5(*c*). There will be only one solution at low Reynolds numbers. This solution is stable. At very low Reynolds numbers there is no solution to (4*b*) because the flow velocities are lower than those of sustainable flames. The flame, however, attaches to the burner tube before these conditions are reached and the discussions of this paper are not applicable.

Figure 6 shows the locus of the solutions of (4*d*) for propane jet issuing from the 0.353 mm diameter tube as a function of the jet Reynolds number. The stable and the unstable branches meet at the critical Reynolds number $Re_{bo}$, beyond which no free-standing flame can be sustained over the jet. The critical Reynolds number is taken as the parameter that determines the blowout condition of the flame. The other interesting flow condition is when the flame stabilizes at $u_x = U_m$. This point is also marked in the figure. The flame is stabilized on the rich branch of the $u_f(C)$ curve for lower Reynolds numbers. Under these conditions the flame has considerable soot formation. Above this flow condition the flame is stabilized on the lean branch of the $u_f(C)$ curve and the flame exhibits very low or no observable soot formation. The flame is blue. A few measurements of the flame stand-off distance are also shown in figure 6. At large stand-off distances the agreement is good. At lower flow rates, however, the flame attaches to the burner as indicated in the figure. The flame exhibits a substantial hysteresis, that is, it is either attached or lifted for the same Reynolds number depending on the history of the flow. This region is also marked in figure 6.

The dependence on the tube diameter of the blowout parameters $x_{bo}$ and $Re_{bo}$ for the propane flame are shown in figure 7. The curves are determined from (13) (or,

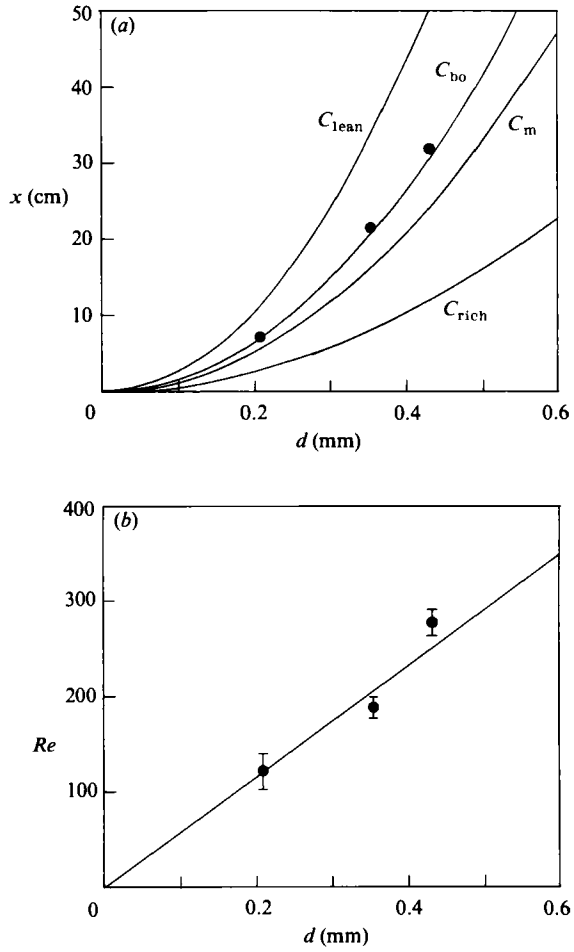


FIGURE 7. Calculated and measured values of the blowout parameters as a function of the burner diameter for propane flame in a round laminar jet discharging from a tube. (*a*) Stand-off distance at blowout $x_{bo}$. (*b*) Reynolds number at blowout $Re_{bo}$.

equivalently, from (14)) using table 1 for the various parameters and are

$$x_{bo} = (1650\ \text{mm}^{-1})\, d^2, \tag{15a}$$

and

$$Re_{bo} = (577\ \text{mm}^{-1})\, d. \tag{15b}$$

The propane concentration at $x_{bo}$ is from (11*c*)

$$C_{bo} = 0.765 C_m, \tag{15c}$$

which is about 1.30 mole/m$^3$. The corresponding laminar flame speed $u_{f,\,bo}$ from either equation (10) or figure 4 as marked is about 36 cm/s, which is significantly lower than the maximum flame speed of 41.7 cm/s. Also shown in figure 7 are the experimentally determined values of $x_{bo}$ and $Re_{bo}$ for the tubes with laminar flow. The blowout Reynolds number was determined by observing the flame at or near the conditions of figure 5 (*b*) where the flame is at the verge of extinction. The flame stand-off distance was determined from both photographs and direct observations. That we could

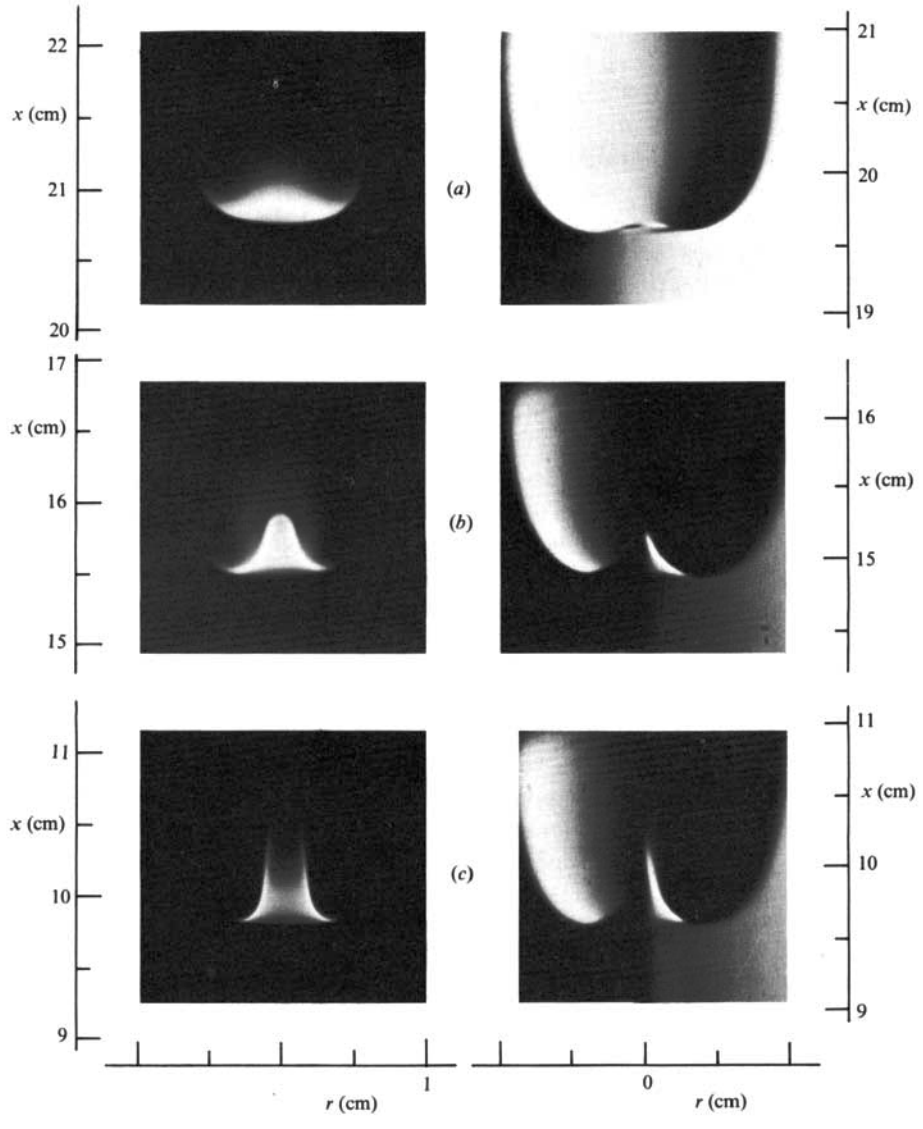


FIGURE 8. Visible (left, $\frac{1}{60}$ s) and schlieren (right, 2.5 μs) pictures of the lifted laminar propane flames over the 0.353 mm diameter tube. (*a*) Just before blowout. (*b*) Near the blowout Reynolds number $Re_{bo} = 201$. (*c*) Below blowout, $Re \approx 160$.

observe and photograph the flame near blowout necessarily implies that even the maxima of the measurements from such observations are lower than the actual flame stand-off distances at blowout. Therefore, we show in figure 7 (*a*) as the measured data the maximum values of the $x_{bo}$ we could observe for various tube burners. The corresponding Reynolds numbers are shown in figure 7 (*b*). The error bars reflect the accuracy of the flowmeter specified by the manufacturer. The agreement between the predicted and the observed values is remarkably good. The downstream location on the jet axis $x_{lean}$ where the local concentration is equal to the lean flammability limit $C_{lean}$ is shown also in figure 7 (*a*). This curve is calculated from (3*b*) at the conditions of (15) as $x_{lean} = (2670\ \text{mm}^{-1})\, d^2$ and is substantially higher than the stand-off

distance at blowout (cf. figure 5*c* and equation (15*a*)). The $C_{\mathrm{m}}$ and $C_{\mathrm{rich}}$ curves are shown also for reference in figure 7(*a*).

Figure 8 shows samples of direct and schlieren photographs of lifted laminar propane flames over the 0.353 mm diameter tubing near and just before blowout. Visible (left, $\frac{1}{60}$ s exposure) and schlieren (right, vertical knife edge, 2.5 μs exposure) pictures taken under comparable conditions are shown side by side in the figure. The flame fronts in figure 8(*a*–*c*) are about 20, 15, and 10 cm downstream from the exit of the tube burner, respectively. If the conventional scaling is used, these flame stand-off distances are about 600, 450, and 300 burner diameters. These large numbers certainly indicate that the flame is in the asymptotic region of the flow and where the details of the burner geometry are no longer relevant. The pictures show the upstream portion of the total flame. The visible flames are blue. The whole flame field has a faint blue envelope which we did not attempt to capture in these pictures as our interest was in the shape of the flame-anchoring region, particularly near blowout conditions. At lower flame stand-off distances, the flame front is highly curved, as evidenced in both the direct and schlieren pictures (figure 8*c*). This curve substantially influences the upstream and lateral flow and temperature fields; therefore, the analysis of the flame front presented above is not satisfactory. As the flame is further lifted, however, the flame front becomes flatter and the assumptions of the analysis of this paper are better satisfied (figure 8*a*). Near blowout the flame front becomes flat; the light intensity diminishes, indicating chemical reactions become weak. Thus, the predictions of the blowout of the analysis presented here should be in good agreement with observations. At the verge of blowout, the flame becomes very sensitive to external disturbances. The disturbance generated by a crisp finger snap, for example, is enough to put out the flame from as far away as 4 metres.

The effects of buoyancy, which were not considered in the theoretical formulation, arise through the non-uniform density field due to the variations in the reactant concentration and through the high temperature combustion products downstream of the flame surface. To check those, we repeated the experiments with various orientations of the pure-fuel jet. We could not observe any significant difference in the values of the blowout parameters and the shape of the flame near blowout until the jet was oriented substantially below the horizontal plane. Only when the jet was pointed vertically downward, did the rising hot flame products change the flame characteristics markedly. Under such conditions the assumptions of the formulation presented in this paper do not apply.

Figure 9 shows the prediction of (4) for the shape of flame front over the 0.353 mm diameter burner at $Re = 200$. The conditions are comparable to those of figure 8(*a*). Both $F_+(\theta)$ and $F_-(\theta)$ start at $R_0 = 183.6$ mm determined from (4*d*), and end on the lean flammability limit surface whose shape is calculated from (3*e*) and (3*f*) with $C = C_{\mathrm{lean}}$. $F_+$ surface curves downstream while $F_-$ surface curves upstream. Although not obvious in the figure, $F_+$ surface has a slightly higher curvature than $F_-$ surface. The two $F$ surfaces have only one common point with the concentration and axial velocity contours passing through $R_0$. The $F_+(\theta)$ surface approximates the outer portions of the observed flame shapes in figure 8. The central parts of the flame, however, seem to conform to a shape much like the local concentration contour. We expect that chemical processes such as fuel pyrolysis and oxidation of soot precursors are dominant in determining the visible shape of the flame there. On the outside, however, the solution $F_+(\theta)$ seems to be a suitable asymptotic form of the flame front in the lean regions of the flame where chemistry ceases to be dominant.

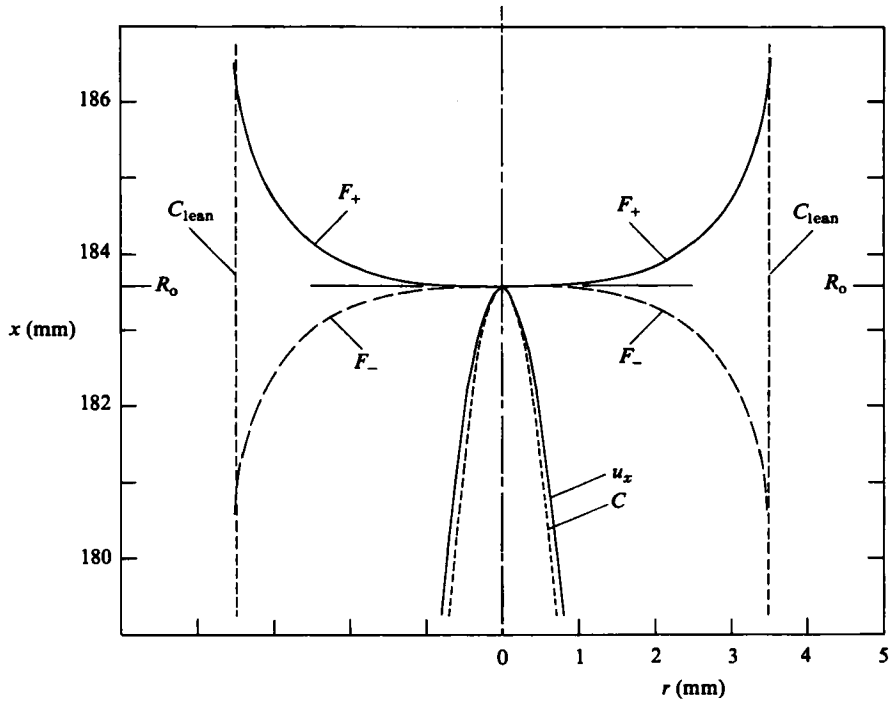


FIGURE 9. Calculated shape $F_+$ of lifted laminar propane flame front over 0.353 mm diameter burner at $Re = 200$ (cf. figure 8*a*). $R_o = 183.6$ mm. Concentration and velocity contours passing through $(R_o, 0)$, $C$ and $u_x$, and the lean flammability limit contour $C_{lean}$ are shown also.

### 7.3. *Hydrogen flame*

Hydrogen was noted to diffuse upstream of the burner in figure 2. Also, table 1 lists the parameters needed in calculating its blowout characteristics even though lifted laminar hydrogen jet flames have not been observed. We could, however, demonstrate the presence of an unstable solution of (4*d*) in the same manner described for propane jet. When the ignition source is moved upstream of that solution, the flame rapidly attaches to the burner. The location of the unstable solution is observed to be much closer to the jet exit plane than that of the propane jet, which is in conformity with predictions (cf. $\gamma = 320$ mm$^{-1}$ for hydrogen and $\gamma = 1650$ mm$^{-1}$ for propane, from table 1). At relatively low flow rates, the hydrogen flame is also observed to move upstream of the exit plane of the jet. The commonly observed axial quenching region near the burner is no longer present. The heating from the flame was seen to be intense enough to heat the stainless-steel burners to glowing red temperatures ($\sim 750$ °C), which confirms the predicted upstream diffusion of hydrogen shown in figure 2. Thus, the experiments substantiate the predictions of the analytical formulation even when the Schmidt number is varied by a factor of nearly 7 from propane to hydrogen.

## 8. Generalization

Even though figure 7 shows for pure propane fuel jet the dependence of the laminar blowout parameters $Re_{bo}$ and $x_{bo}$ on the burner-tubing diameter $d$, a general presentation is possible if the data are presented in the dimensionless forms suggested by (11). In fact, such a presentation must be universal inasmuch as the laminar flame

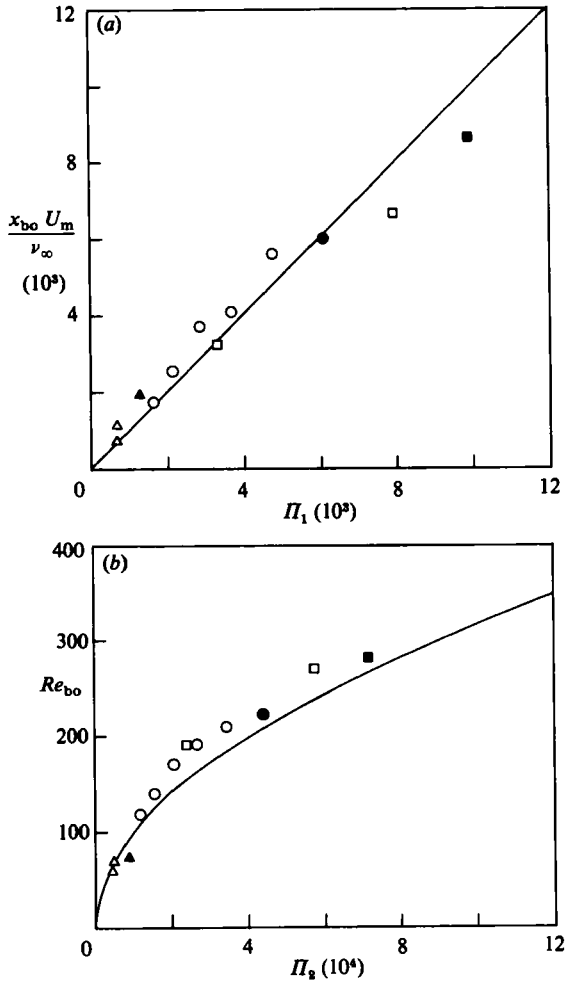


FIGURE 10. Laminar blowout parameters $x_{bo}$ and $Re_{bo}$ for pure and diluted propane jet flame as functions of the fuel properties and molar fuel flow rate. Solid symbols, pure propane jet; open symbols, diluted with air. Triangles, 0.208 mm burner; circles, 0.353 mm burner; squares, 0.453 mm burner. Fuel jets were diluted up to 45% fuel by volume. (*a*) Blowout height $x_{bo}$, data and (11*a*). (*b*) Blowout Reynolds number $Re_{bo}$, data and (11*b*).

speed $u_f(C)$ of fuel gases can be approximated by (10). Further, since the amount of fuel in the flow field enters this presentation through the molar fuel flow rate $N$, if the jet fluid is not pure, but diluted with the ambient gases or with gases whose presence do not alter significantly the shape of the $u_f(C)$ characteristics of the fuel–oxidizer combination, the predictions of (11) for the blowout of laminar lifted flames must remain valid. These arguments can easily be tested.

The two plots of figure 10 show the results of various experiments in the coordinates suggested by (11). The dimensionless flame stand-off distance at blowout $U_m x_{bo}/\nu_\infty$ and the corresponding Reynolds number $Re_{bo}$ are shown as functions of the two dimensionless groups

$$\Pi_1 = \frac{1}{8\pi}\frac{2Sc+1}{1-\beta}\frac{U_m N_{bo}}{\nu_\infty^2 C_m},$$

and $$\Pi_2 = \tfrac{2}{3}\alpha\beta(2Sc+1)\frac{U_m N_{bo}}{\nu_\infty^2 C_m},$$

respectively. These two dimensionless groups which are derived from the analytic solution of the phenomenon, scale the fuel flow rate at blowout $N_{bo}$ with the diffusion and combustion properties of the particular fuel–oxidizer combination through the Schmidt number $Sc$; the laminar flame speed properties of $U_m$, $C_m$, $\alpha$, and $\beta$; and the kinematic viscosity of the ambient fluid $\nu_\infty$. Typical numerical values for numerous parameters needed for the construction of $\Pi_1$ and $\Pi_2$ are listed in table 1 for some fuels.

Data for pure propane are indicated with solid symbols for various diameters of burner. The open symbols indicate the data for fuel jets diluted with air in a continuous-flow apparatus. Two identical flowmeters were used to measure the relative flow rates of the fuel gas and air before they were mixed. The readings from these two flowmeters are used to determine the partial fuel density in the jet fluid $\rho_f$. The jets were diluted to as low as 45% fuel by volume. The jet Reynolds number $Re_{bo}$ and the molar fuel flow rate $N_{bo}$ are then determined using (12*b*) and (12*c*). The agreement between the measured values and the predictions of (11) are good for low Reynolds numbers where the jet flow is hydrodynamically stable. At higher Reynolds numbers, however, the flow-field instabilities, which are extremely sensitive to even minute disturbances in the environment, make the $x_{bo}$ measurements rather difficult, while the blowout Reynolds number $Re_{bo}$ could be ascertained with relatively less difficulty. Given the inherent uncertainties in the values in table 1 and the difficulties involved in any kind of stability experiment, the data of figure 10 confirm reasonably well the applicability of the arguments presented here. The recent arguments of Broadwell *et al.* (1985) suggest somewhat similar phenomena occur in turbulent flames.

## 9. Concluding remarks

The exact solution of the concentration field of a round laminar jet is presented. This solution shows the explicit dependence of the concentration field on the Schmidt number. The corresponding laminar boundary-layer equations are not adequate for the description of fields with low Schmidt numbers. The concentration field and the laminar flame speed characteristics of fuel discharging from a small orifice are combined into a kinematic argument to calculate the shape of the base of the lifted laminar flame. A formal criterion is proposed for the spatial stability of the flame front. The condition for the existence of the flame front gives a general criterion for the blowout of the lifted laminar flame. With a second-order curve fit to the existing flame-speed data, an explicit relationship between various flow and fuel parameters is established for the blowout of the lifted laminar flame. This formulation does account for the diluted fuel jets also. Simple experiments were performed to verify the predictions of flame shape and stability. The observed flame shape and stability characteristics of both pure and diluted propane jets were found to be in good agreement with the predictions. Thus, the blowout phenomenon can be accounted for from the fluid-mechanics arguments alone.

The ideas developed in this paper are equally applicable to the flame over a laminar oxidizer jet discharging into a fuel gas. The flame blowout occurs on the rich flammability branch of the particular $u_f(C)$ curve; therefore, a curve fit analogous to (10) to that part of the flame-speed curve is needed to evaluate constants similar to

$\alpha$ and $\beta$. Although the discussions of this paper are confined to laminar flames, it would be an interesting endeavour to explore their extension to lifted turbulent flames and, in particular, the applicability of the dimensionless variables similar to $\Pi_1$ and $\Pi_2$ to the description of the blowout of turbulent flames.

This research is being supported by the National Science Foundation under Grant No. CBT 84 03781. We would like to thank R. F. Huang and J. L. Rodriguez Azara for their assistance.

## REFERENCES

ANDREWS, G. E. & BRADLEY, D. 1972 The burning velocity of methane–air mixtures. *Combust. Flame* **19**, 275–288.

BARR, J. 1953 Diffusion flames. *Fourth Symposium (Intl) on Combustion*, pp. 765–771.

BATCHELOR, G. K. 1967 *An Introduction to Fluid Dynamics*. Cambridge University Press.

BOTHA, J. P. & SPALDING, D. B. 1954 The laminar flame speed of propane/air mixtures with heat extraction from the flame. *Proc. R. Soc. Lond.* A **225**, 71–96.

BROADWELL, J. W., DAHM, W. J. A. & MUNGAL, M. G. 1985 Blowout of turbulent diffusion flames. *Twentieth Symposium (Int.) on Combustion*, pp. 303–310.

EGERTON, A. & THABET, S. K. 1952 Flame propagation: the measurement of burning velocities of slow flames and the determination of limits of combustion. *Proc. R. Soc. Lond.* A **211**, 445–480.

EICKHOFF, H., LENZE, B. & LEUCKEL, W. 1985 Experimental investigation on the stabilization mechanism of jet diffusion flames. *Twentieth Symposium (Intl) on Combustion*, pp. 311–318.

GIBBS, G. J. & CALCOTE, H. F. 1959 Effect of molecular structure on burning velocity. *J. Chem. Engng Data* **4**, 226–237.

KANURY, A. M. 1977 *Introduction to Combustion Phenomena*, 3rd edition. Gordon & Breach.

LANDAU, L. D. 1944 A new exact solution of the Navier–Stokes equations. *Dokl. Akad. Sci. URSS* **43**, 286–288.

LANDAU, L. D. & LIFTSHITZ, E. M. 1959 *Fluid Mechanics*. Pergamon.

PETERS, N. 1985 Partially premixed diffusion flamelets in non-premixed turbulent combustion. *Twentieth Symposium (Int.) on Combustion*, pp. 353–360.

PETERS, N. & WILLIAMS, F. A. 1983 Liftoff characteristics of turbulent jet diffusion flames. *AIAA J.* **21**, 423–429.

SAVAŞ, Ö. & GOLLAHALLI, S. R. 1986 Flow structure in near-nozzle region of gas jet flames. *AIAA J.* (in press).

SCHOLEFIELD, D. A. & GARSIDE, J. E. 1949 The structure and stability of diffusion flames. *Third Symposium (Intl) on Combustion*, pp. 102–110.

SIVASHINSKY, G. I. 1983 Instabilities, pattern formation, and turbulence in flames. *Ann. Rev. Fluid Mech.* **15**, 179–199.

SQUIRE, H. B. 1951 The round laminar jet. *Q. J. Mech. Appl. Maths* **4**, 321–329.

TAKAHASHI, F., MIZOMOTO, M. & IKAI, S. 1983 Laminar burning velocities of hydrogen/oxygen/inert gas mixtures. In *Alternate Energy Sources* (ed. T. N. Veziroğlu), vol. 5, pp. 447–457. Hemisphere.

TAKAHASHI, F., MIZOMOTO, M., IKAI, S. & FUTAKI, N. 1985 Lifting mechanism of free diffusion flames. *Twentieth Symposium (Intl) on Combustion*, pp. 295–302.